

# Excitonic complexes in MOCVD-grown GaAs-based quantum dots emitting at telecom wavelengths

Paweł Mrowiński<sup>1</sup>, Anna Musiał<sup>1,†</sup>, Krzysztof Gawarecki<sup>2</sup>, Łukasz Dusanowski<sup>1,\*</sup>, Tobias Heuser<sup>3</sup>, Nicole Srocka<sup>3</sup>, David Quandt<sup>3</sup>, André Strittmatter<sup>3,\*\*</sup>, Sven Rodt<sup>3</sup>, Stephan Reitzenstein<sup>3</sup>, and Grzegorz Sęk<sup>1</sup>

<sup>1</sup>*Laboratory for Optical Spectroscopy of Nanostructures, Department of Experimental Physics, Faculty of Fundamental Problems of Technology, Wrocław University of Science and Technology, Wybrzeże Wyspiańskiego 27, 50-370 Wrocław, Poland*

<sup>2</sup>*Department of Theoretical Physics, Faculty of Fundamental Problems of Technology, Wrocław University of Science and Technology, Wybrzeże Wyspiańskiego 27, 50-370 Wrocław, Poland*

<sup>3</sup>*Institute of Solid State Physics, Technical University of Berlin, Hardenbergstraße 36, D-10623 Berlin, Germany*

*\*Present address: Technische Physik, University of Würzburg, Am Hubland, D-97074 Würzburg, Germany*

*\*\*Present address: Institute of Experimental Physics, Otto von Guericke University Magdeburg, D-39106 Magdeburg, Germany*

Hereby, we present a comprehensive experimental and theoretical study of the electronic structure and optical properties of excitonic complexes in strain-engineered InGaAs/GaAs quantum dots (QDs) grown by metal-organic chemical vapour deposition and emitting at the 1.3- $\mu\text{m}$  telecommunication window. Binding energies of excitonic complexes as well as the fine structure of the neutral exciton including dark excitonic states are determined experimentally by means of polarization-resolved microphotoluminescence and magneto-spectroscopy. Experimental results on a number of single quantum dots of an inhomogeneously broadened QD ensemble are compared with the results of electronic structure modelling employing the 8-band  $k\cdot p$  theory combined with the configuration interaction method. Realistic system parameters including QD geometry and composition gradients have been used following the cross-sectional structural data, which allowed for a quantitative agreement between the experimental data and the theoretical results. Understanding the influence of structural parameters as QD size and compositions, of both, the nanostructure itself and the neighboring strain reducing layer, shows which of them are crucial to control the emission wavelength and to achieve the telecommunication spectral range and which on the other hand, affect predominantly the energy separation of the ground state excitonic complexes. The main determinant of the exciton ground state energy and the binding energies of excitonic complexes including their energetic order appeared to be the indium composition in the QDs. In contrast, variation of both the QD size or composition of the strain reducing layer was not able to reproduce the experimental tendencies properly. The results allow gaining deeper knowledge on limitations of the investigated structures in terms of good spectral isolation of individual optical transitions, the spatial confinement regime and thermal stability of emission from individual QD states. All these features and relations are crucial in view of QD applications in single-photon sources of high purity at telecom wavelengths.

**PACS number(s):** 78.30.Fs III-V and II-VI semiconductors; 78.67.-n Optical properties of low-dimensional, mesoscopic, and nanoscale materials and structures; 78.67.Hc Quantum dot; 73.22.-f Electronic structure of nanoscale materials and related systems;

## I. INTRODUCTION

Semiconductor nanostructures have become a powerful and flexible technology platform to study quantum optics phenomena in the solid state.<sup>1</sup> The main advantage of solid-state structures with quantum dots (QDs) in comparison to atomic systems is their compactness and the possibility to tailor their selected properties for a specific application. To optimize QDs for novel quantum technologies such as, e.g., quantum communication networks, it is crucial to perform comprehensive studies of their optical properties and underlying electronic structure as well as identify their determining factors by means of excitonic and excited state spectra, in particular on the level of a single quantum emitter. With respect to practical applications in fiber-based quantum communication it is of great importance to develop QD-based non-classical light sources emitting in the telecommunication spectral ranges (1.3 and 1.55  $\mu\text{m}$ ). One of the approaches to target this challenge is to use GaAs-based QDs and redshift their emission (typically centered at 900-1050 nm at 10 K for InGaAs/GaAs QDs) towards the telecommunication range. If compared to InP-based approaches<sup>2-5</sup> it combines the advantage of mature fabrication and material processing of GaAs-based technology with compatibility and straightforward integration. Additionally, fabrication of high-quality distributed Bragg reflectors (DBRs) to enhance the extraction efficiency of the QD emission and also microcavities are much less demanding in GaAs-based structures in comparison to InP-based due to availability of compatible materials with high refractive index contrast. Various methods have been explored to reach the telecom range in this material system by: (i) engineering the strain in InAs/GaAs QDs utilizing an InGaAs strain reducing layer (SRL)<sup>6-10, 11-14</sup> (ii) by using SRL containing Sb for deeper confining potential;<sup>15-18</sup> (iii) deposition of the InAs QDs on InGaAs metamorphic buffer layers;<sup>19,20</sup> (iv) using bilayers of differently-sized QDs where the first layer acts as a seeding layer and modifies the strain conditions for the second one;<sup>21-24</sup> (v) increasing the QD height by growth up to the second critical thickness;<sup>25,26</sup> (vi) increasing the QD size using atomic layer molecular-beam epitaxy (MBE);<sup>27</sup> (vii) using activated alloy phase separation<sup>28</sup> or (viii) nitridation of InAs/GaAs QDs leading to formation of dilute nitride InAsN QDs.<sup>29</sup> It is especially desirable to obtain emission around the 1310 nm spectral window due to lack of dispersion and local minimum of losses for the standard fiber networks which is achievable in the GaAs-based structures and suitable for applications in local networks for short- and medium-range communication. The alternative material system providing emission at telecom wavelengths could be InAs on InP, but in that case it is rather optimized for longer wavelengths of 1550 nm and covers the range of absolute minimum of losses preferential for long-haul data transmission, but on the expense of possible distortion of the optical signal due to dispersion.

In this paper we investigate fundamental physical properties of excitonic complexes confined in InGaAs/GaAs QD structures capped with InGaAs strain reducing layer of lower In content, in view of their practical implementation in non-classical light sources for short range quantum communication protocols at the telecom O-band.<sup>30</sup> The quality of these structures have reached the level enabling systematic experimental study on many QDs, but their practical application still requires optimization as the structural quality and therefore the internal quantum efficiency of the emitters is not yet comparable to their counterparts emitting at shorter wavelengths. Ensembles of such structures with high spatial density have already been investigated in view of laser applications with the focus on the role of the SRL in redshifting the QDs' emission towards

telecommunication wavelengths on the level of the averaged optical response.<sup>9,31,32</sup> Here, we focus on single quantum emitters and identifying their optical and electronic properties including the exciton fine structure, the dark excitonic states as well as the binding energies of excitonic complexes in function of emission energy and morphological parameters. This enables us to pinpoint efficient single optical transitions of good thermal stability. We study both experimentally and theoretically the properties of various excitonic complexes by means of microphotoluminescence ( $\mu$ PL), also in magnetic field, and compare them with 8-band  $k$ - $p$  modelling<sup>33</sup> combined with the configuration interaction proven to reflect properly the excitonic states in different types of epitaxial QDs.<sup>34,35</sup> The obtained results on the single-particle states and binding energies of excitonic complexes with respect to such system parameters as QD geometry and composition as well as SRL composition are critical for proper understanding of this group of nanostructures and the interdependence between the structural properties, electronic structure and the resulting optical properties of single QDs of that kind grown by metal organic chemical vapor deposition (MOCVD), which is relatively cheap and efficient technique compared to other epitaxial growth methods. They also provide means for understanding and tailoring the electronic structure and optical properties for specific single QD-based applications while maintaining their emission in the O-band fiber window. So far, similar QD structures with however different structural properties and ultra-low spatial density were studied with respect to cascaded emission of photons (from both neutral and charged excitonic complexes)<sup>14</sup> and temperature dependence of photoluminescence<sup>36</sup> followed by demonstration of single-photon emission.<sup>37</sup> However, these structures exhibit mainly negative charged complexes, whereas in those investigated in this work positive trions are preferentially formed suggesting a significantly changed excitonic spectrum due to different morphological properties. The study on the optical properties of similarly fabricated structures presented so far in the literature concerns only the fine structure splitting of the neutral exciton,<sup>11</sup> but not the binding energies of the multicarrier excitonic complexes, nor their interplay with the ground state emission energy as well as energetic order of the respective excitonic complexes. Therefore, this is the main focus of the current work. In addition, we also extend the existing knowledge by direct detection of dark excitonic states in these nanostructures which has not been reported before. This is fully complementary analysis to the recent comprehensive study on structural and optical properties of GaAs-based QDs on metamorphic buffer layer for emission at longer wavelengths of the telecom C-band<sup>38</sup> for which emission of single photons and entangled photon pairs has been demonstrated.<sup>39,40</sup>

The paper is organized as follows: Section II provides details on the investigated structures together with a description of the utilized experimental setups. In Section III experimental findings are discussed whereas Section IV presents the quantum dot model used in theoretical calculations together with the obtained results and their comparison to experiments. Section V concludes the paper.

## II. INVESTIGATED STRUCTURES AND EXPERIMENTAL SETUP

The investigated epitaxial heterostructure containing self-assembled  $\text{In}_x\text{Ga}_{1-x}\text{As}$  on GaAs QDs was grown by MOCVD in the Stranski-Krastanow growth mode. QDs on a wetting layer are formed of  $\text{In}_{0.75}\text{Ga}_{0.25}\text{As}$  (0.7 nm of the nominal deposited material). The QDs of  $\sim 10^9/\text{cm}^2$  areal density are covered by a low-indium content  $\text{In}_{0.2}\text{Ga}_{0.8}\text{As}$  SRL, purpose of which is to redshift the ground state transition energy to the telecom spectral range.<sup>31,41</sup> For enhanced extraction efficiency of the emitted radiation, QDs are grown on a distributed Bragg reflector (DBR) composed of 23 pairs of GaAs/AlGaAs layers (101.6/115.4 nm thickness measured by scanning

electron microscopy - SEM) on top of the undoped GaAs buffer (300 nm). The thickness of the GaAs layer surrounding the QD layer is designed to form a  $2\lambda$  cavity between the DBR and the surface [Fig 1(a)]. Additionally, cylindrical mesa structures of various diameters in the range of 300 nm to 2100 nm and 670 nm height were fabricated in a regular pattern using electron-beam lithography performed at room temperature followed by reactive-ion etching (ICP-RIE) [inset in Fig. 1(b)]. Such mesas provide increased spatial resolution by removing neighboring QDs and thus their contribution to the background emission. Moreover, it limits the losses of optical signal to the sides important in  $\mu$ PL experiments [Fig. 1(b)]. It has been shown theoretically that optimized mesa design can lead to extraction efficiencies comparable to those achievable with microlenses, but it is more robust against fabrication imperfections<sup>42</sup> which has also been confirmed experimentally within deterministic technology platforms.<sup>43,44</sup>

All the presented microphotoluminescence results are obtained for the described sample mounted in a liquid helium continuous-flow cryostat (at 5K) and under non-resonant continuous wave (cw) excitation at 660 nm. The excitation is delivered to the sample and the signal is collected via a long working distance microscope objective with 0.4 numerical aperture. The signal is further spectrally resolved by a 1-m focal length monochromator with a 600 grooves/mm grating and detected using a multichannel liquid nitrogen-cooled InGaAs linear detector. The setup provides a spectral resolution of at least 25  $\mu$ eV and spatial resolution of about 1  $\mu$ m. For polarization-resolved measurements, we used a rotating half-wave plate and a linear polarizer adjusted for the maximal transmission of the experimental setup. The magneto-optical study was performed using a microscopy cryostat with superconducting coils generating magnetic fields up to 5 T which allows for measurements in both, Voigt and Faraday configurations. For photon auto- and cross-correlation measurements, we utilized a free-space Hanbury Brown and Twiss (HBT) setup with a non-polarizing 50:50 beam splitter and two 0.32 m focal length monochromators used as spectral filters and a pair of superconducting NbN nanowire single-photon counting detectors with  $\sim 20\%$  quantum efficiency and 10 dark counts/s at 1.3  $\mu$ m. The photon correlation statistics was acquired by single-photon correlation electronics giving an overall temporal resolution of the HBT setup of 80 ps.

### III. EXPERIMENTAL RESULTS AND DISCUSSION

The optical properties of the investigated QDs have been examined by performing high-resolution  $\mu$ PL experiments in function of excitation power, linear polarization and magnetic field. The representative emission spectrum indicating a set of lines from a single QD in a circular mesa structure of 1300 nm in diameter is shown in Fig 2(a). It presents two spectra measured for polarization along the [110] and [1-10] in-plane crystallographic directions. Based on the excitation power dependence [Fig 2(b)], the full scan of polarization angle [Fig 3(a)] and photon cross-correlation measurements [Fig 4(a)] one can unambiguously identify the characteristic features as the neutral exciton (X) and the biexciton (XX): i) the fine structure splitting (FSS) is opposite for XX and X in terms of the energetic order of the polarized components, ii) expected approximately linear and quadratic excitation power dependence of the emission intensity in the low excitation limit for X and XX, respectively and iii) anti-bunching followed by bunching as a signature of cascaded emission in the cross-correlation of photon-emission events from X and XX [Fig. 4(a)]. On the other hand, the lack of the spectral splitting in the polarization-resolved study, the sublinear emission intensity dependence on excitation power and a quadruplet

splitting observed in the in-plane magnetic field indicates the charged complex character of the other QD emission lines (labelled as  $X^+$ ,  $X^-$  in Fig. 2). Furthermore, we found indications of emission from probably the higher order excitonic states of the positively charged branch as  $X^+_T$  and  $XX^+_T$  having inverted spectral patterns with two linearly polarized components and the splitting of about 350  $\mu\text{eV}$  between them,<sup>45</sup> as well as showing sublinear and superlinear emission intensity dependence on excitation power [Fig. 2(b)]. The positively charged character of the QD is mainly attributed to unintentional p-doping in the MOCVD growth process, which is also indicated by a higher emission intensity of  $X^+$  than  $X^-$  and  $X$ , in contrast to existing reports demonstrating rather negatively-charged character.<sup>14</sup> The other observed spectral features could be related to excited states and higher-order excitonic complexes including carriers in the p-shell states as reported previously for more common InAs/GaAs system<sup>46,47</sup> or emission from a different QD located in the same mesa. Additionally, for the  $X$  line an auto-correlation of photon emission events under non-resonant cw excitation was measured [Fig. 4(b)]. The of the second-order correlation function at zero delay gives the as measured value of  $g^{(2)}(0) = 0.17$  and  $g^{(2)}(0) = 0.05$  after deconvolution with temporal response of the experimental setup, which proves the single-photon character of the source. The non-ideal value is attributed to uncorrelated background emission either due to multiple QDs in a mesa for this spatial QD density or emission from defects in the structure (most probably in the substrate).

The identification of excitonic complexes of the single QD under study allows us to determine their binding energies to be:  $\Delta E_{X^+} = -1.7$  meV,  $\Delta E_{X^-} = -3.5$  meV and  $\Delta E_{XX} = -3.7$  meV, for,  $X^+$ ,  $X^-$  and  $XX$ , respectively, being in the range of values similar to MBE-grown QDs<sup>35,48</sup> and low-density MOVPE-grown QDs<sup>14</sup> in this material system emitting below 1  $\mu\text{m}$  wavelength. The FSS of the neutral exciton (60  $\mu\text{eV}$ ) is also rather typical for In(Ga)As/GaAs (001) QDs emitting below 1  $\mu\text{m}$  wavelength,<sup>49</sup> which has not been optimized in terms of minimizing the FSS. In order to obtain the splittings of the bright-dark and dark-dark spin configurations we collected also the magneto-optical data. Figure 3(b) shows the emission spectra from the same QD with features from various excitonic complexes influenced by an external in-plane magnetic field of 5 T (Voigt configuration). It allows us to observe the dark excitonic states due to their mixing with bright excitonic states. By extrapolating the energies of the respective excitonic components down to zero magnetic field, one can determine both the bright-dark and dark-dark  $X$  splittings.<sup>50</sup> This procedure enables us to identify the zero-field energy of the dark states, and hence the bright-dark splitting of 430  $\mu\text{eV}$  and dark-dark splitting of approx. 20  $\mu\text{eV}$  were determined. Additionally, the quadruplet splitting of the charged excitons allows determining the in-plane  $g$ -factors of electron and hole yielding  $g_{e,\perp} = 0.99$  and  $g_{h,\perp} = 0.28$ . A non-zero in-plane hole  $g$ -factor suggests slight contribution of the light-hole states to the valence band ground state, which can result from an intrinsic anisotropy of the confining potential due to, e.g., the QD shape anisotropy or inhomogeneous (piezoelectrically-induced) strain around the QD. A fingerprint of the presence of the valence-band mixing is also seen in the non-zero polarization anisotropy of the exciton emission of about 5% in agreement with rather low asymmetry of in-plane QD shape when based on structural data.

In the next step, we performed the same analysis as the exemplary one presented in Figs. 2 and 3 for several QDs embedded in similar mesa structures, in order to gather the statistics and to examine the  $X$  emission energy dependence of the exciton FSS and the binding energies of the excitonic complexes. The obtained results are presented in Fig. 5. The histogram of exciton FSS [inset in Fig. 5(a)] shows a distribution from 30  $\mu\text{eV}$  to

85  $\mu\text{eV}$  with a pronounced maximum at 65  $\mu\text{eV}$ . At the same time, there is no clear X energy dependence of the exciton FSS probably due to several factors contributing to the exciton energy<sup>51</sup> - see the discussion below.

In the case of the binding energies of basic excitonic complexes [Fig. 5(b)], we observe a large scattering for the XX and  $X^-$  (with however some general trends indicated by the guide to the eye) and a rather weak dependence as a function of the X energy, whereas a clear decrease of the binding energy of the  $X^+$  complex with increasing exciton energy is observed. The scattering of the data for the XX and  $X^-$  binding energy is probably due to less localized electron wave function as compared to the hole counterpart making these binding energies more sensitive to changes in In composition and its distribution influencing simultaneously the band-gap potential and effective masses, and thus direct Coulomb interactions and correlation effects.<sup>35</sup> At the same time, a rather smooth  $X^+$  binding energy dependence can be related to a more localized hole wave function [see also Fig. 7(b)] and according to the results of k-p modelling (see details below) it is most probably driven by the In content. Perhaps, the same fluctuations of the confinement potential being related to the QD composition could be also responsible for the FSS distribution.<sup>52,53</sup>

#### IV. THEORETICAL MODEL AND RESULTS

In this section, a model of the QD as well as details of the methods utilized to calculate the electronic/excitonic structure are presented. We assume realistic shape of the dot<sup>54</sup> by describing its upper surface as:

$$Z(x, y) = h \exp\left[-\left(\frac{x^2 + y^2}{r_b^2}\right)^2\right], \quad (1)$$

where  $h$  denotes the height and  $r_b$  is an in-plane extension parameter related to the base size. The dot is placed on a  $h_{\text{WL}}$  thick  $\text{In}_{0.75}\text{Ga}_{0.25}\text{As}$  wetting layer (WL). The material distribution in the system is shown in Fig. 6(a) for our model QD design. Fig. 6(b) shows a transmission electron microscopy (TEM) cross section of a representative QD. There is presented the spatial mapping of the real part of the interference between the  $\{000\}$  and  $\{200\}$  (in-plane direction) beams. Within the approximate specimen thickness of  $\sim 50$  nm this quantity is monotone with the projected In concentration along the electron beam thus given a qualitative impression of the QD shape. However, from this TEM data it is not possible to deduce the specimen thickness and thus the absolute value of the In content within a certain cross-sectional plane. Based on that image we assume a gradient material distribution inside the QD. To determine the In content the sample was investigated under a  $21.7^\circ$  out of the  $[010]$  plane rotation angle (not shown here). In that case, the sample thickness can be estimated from reflex positions of the WL, the QDs are modeled as hemispheres, the SRL thickness is neglected, and the In content can be calculated. The selected QD has an In content of  $(77 \pm 13) \%$ . Therefore, in the QD model the local In content changes from  $C_{\text{max}}$  to  $C_{\text{min}}$  within the assumed QD shape, i.e.  $0 \leq z \leq Z(x, y)$ , according to the dependence

$$C(x, y, z) = C_{\text{min}} + (C_{\text{max}} - C_{\text{min}}) \exp\left(-\frac{x^2 + y^2}{r_0^2}\right) \exp\left(-\frac{(z - z_c)^2}{z_0^2}\right), \quad (2)$$

here  $r_0$ ,  $z_0$  define spatial extensions and  $z_c$  is related to the position of the gradient. The parameter set for a representative QD (optimized according to the experimental results on the QD ensemble – average values) is given by:  $h = 6$  nm,  $r_b = 15$  nm,  $h_{\text{WL}} = 0.6$  nm,  $C_{\text{max}} = 0.95$ ,  $C_{\text{min}} = 0.5$ ,  $r_0 = 12$  nm,  $z_0 = 6$  nm,  $z_c = h/2$ . This gives an average In content inside the dot of  $C_{\text{avg}} = 0.727$  similar to obtained based on the structural data. The strain

reducing layer far aside a QD has a constant thickness equal to the nominal value of  $h_{\text{SRL}} = 4.2$  nm and In content  $C_{\text{SRL}} = 0.2$ . On the other hand, in the QD vicinity, we assume its upper surface is given by Eq. 1 with  $h \rightarrow h'_{\text{SRL}} = 7.8$  nm,  $r_b \rightarrow r'_{\text{SRL}} = 30$  nm. The lattice mismatch between InGaAs and GaAs results in a strain field, which affects the band structure. We calculate the strain distribution in the system within a continuous elasticity approach.<sup>55</sup> The piezoelectric field is accounted for by taking a strain-induced polarization up to the second order.<sup>56</sup> The electron and hole single-particle states are calculated within the 8-band  $k \cdot p$  method.<sup>57</sup> Further details of the calculations as well as the material parameters are presented in Ref. [58].

The total Hamiltonian of the system in the picture of second quantization is given by

$$H = \sum_n \epsilon_n^{(e)} a_n^\dagger a_n + \sum_m \epsilon_m^{(h)} h_m^\dagger h_m - \sum_{nn'mm'} V_{nmm'n'}^{(e-h)} a_n^\dagger h_m^\dagger h_m a_{n'} + \frac{1}{2} \sum_{nn'mm'} V_{nn'mm'}^{(e-e)} a_n^\dagger a_m^\dagger a_{m'} a_{n'} + \frac{1}{2} \sum_{nn'mm'} V_{nmm'n'}^{(h-h)} h_n^\dagger h_m^\dagger h_m h_{n'},$$

where  $\epsilon_n^{(e)}$  ( $\epsilon_m^{(h)}$ ) are the energies of the electron (hole) states found from 8-band  $k \cdot p$  calculations,  $a_n^\dagger$ ,  $a_n$  ( $h_m^\dagger$ ,  $h_m$ ) are operators of creation and annihilation of electrons (holes) in state  $n$  ( $m$ ). The Coulomb integrals are defined by

$$V_{nmm'n'}^{(e-h)} = \frac{e^2}{4\pi\epsilon_0\epsilon_r} \int d\mathbf{r} \int d\mathbf{r}' \Psi_n^{\dagger(e)}(\mathbf{r}) \Psi_m^{\dagger(h)}(\mathbf{r}') \frac{1}{|\mathbf{r}-\mathbf{r}'|} \Psi_{m'}^{(h)}(\mathbf{r}') \Psi_{n'}^{(e)}(\mathbf{r}),$$

where  $e$  denotes the electron charge and  $\epsilon_0$ ,  $\epsilon_r$  are vacuum permittivity and relative dielectric constant for GaAs.  $\Psi_n^{(e)}(\mathbf{r})$  ( $\Psi_m^{(h)}(\mathbf{r}')$ ) are 8-component spinors related to the electron (hole) eigenstates. An analogous definition is used in the case of  $V_{nm}^{(e-e)}$  and  $V_{nmm'n'}^{(h-h)}$ .

To find exciton, trion and biexciton states we use the configuration interaction approach. We take into account a basis of 40 electron and hole states (including spin degeneracy) which gives 1 600 exciton, 31 200 trion and 608 400 biexciton configurations. The resulting matrices for trions and biexciton are sparse and they are diagonalized using the SLEPC library.<sup>59</sup> The importance of the correlations in the investigated system can be illustrated by showing the binding energies of excitonic complexes in function of the number of states included in the calculations [Fig. 9]. Convergence tests reveal that the correct description of long-wavelength InGaAs/GaAs QDs indeed requires modelling beyond the Hartree-Fock approximation to properly describe the states of the investigated system.

In order to model the QD electronic structure and to verify the assumed system parameters, the emission spectrum of a QD was calculated and compared to the experimental results presented above. In the first step, a single-particle energy level spectrum [Fig. 7(a)] and wave functions [Fig. 7(b)] were calculated. The in-plane carrier density probability distribution has a high symmetry as a QD shape and In composition with cylindrical symmetry have been assumed following the low degree of linear polarization of exciton emission observed in the optical experiments. Due to a strongly inhomogeneous In distribution [Fig. 6] in the QD volume, the wave function extension is smaller than the physical size of the QD and so the confinement is actually effectively stronger than one might expect from the dimensions of the QD itself. Figure 8 shows that the fundamental properties of the investigated system are well reproduced by the calculations. In Figure 8(a) high-excitation spectra of the QD ensemble, exhibiting emission also from higher QD energy states (upper panel), are compared to the calculated excitonic spectrum (lower panel): the splitting between the ground state and the first higher

energy state (p-shell) equals to 75 meV in both experiment and theory. Figure 8(b) presents the binding energies of basic excitonic complexes: calculated (black solid line for QD  $r_b = 15$  nm,  $h = 6$  nm, In content in SRL of 20 %, average In content in QD of 73 %, X energy - 0.95708 meV) and determined experimentally [red arrows, X energy 0.95719 eV – Fig. 5(b)]. For the sake of this comparison, an experimental example with matching exciton emission energy was chosen and furthermore the exciton energy was subtracted from both experimental and calculated data. The calculated binding energies of the excitonic complexes in this yielded: -0.98 meV, -1.97 meV and -2.29 meV for  $X^+$ , XX and  $X^-$ , respectively. The ordering of the excitonic complexes in the spectrum and their relative binding energies are in good agreement with the experimentally obtained values with a systematic shift (underestimating the binding energies) due to the fact that exchange interaction correction is not included in these calculations and the parameters were chosen to reproduce average properties of the QD ensemble.

In the case of the experiment, we do not have access to the exact structural information for an individual QD studied optically, but we do have the spectral distribution of the main properties measured for various dots. It is then possible to determine the interdependence of QDs' optical properties as a function of X emission energy, but there might be multiple interdependent factors causing the change of X energy. Because of that a detailed study was performed exploring the influence of the QD's size and the average In composition in the QD and SRL on the binding energies of the excitonic complexes (Fig. 10). These results reveal that the size of the QD has rather weak influence on the binding energies of the  $X^+$ , whereas binding energies of XX and  $X^-$  change by about 400  $\mu$ eV when the ground state energy is shifted by almost 100  $\mu$ eV due to the size effect [Fig. 10(a)]. On the other hand, the In content in the QD has a strong impact on the binding energies of the trions and it leads to their crossing for low average In content and so to reordering of the excitonic complexes' appearance in the emission spectrum [Fig. 10(b)]. The value of the binding energy of the positive trion ( $X^+$ ) decreases (i.e. its absolute value) from -2.4 meV for low In content to -0.91 meV for high In content evidencing that it is crucial to obtain isolated emission lines from a single QDs also at long wavelengths. Additionally, a crossing of negative trion ( $X^-$ ) and biexciton (XX) binding energies can be found in these results showing that the In content fluctuations can lead to a reordering of these lines, which is consistent with the experimental results discussed in Sec. III. At the same time, the average QD composition strongly influences the ground state energy, and a high In content is indispensable to maintain the emission in the telecom range and to reproduce the experimental results. The same is true for the In composition of the SRL, i.e. it mainly influences the ground state energy, but has rather weak impact on the binding energies of the excitonic complexes [Fig. 10(c)]. When a QD structure with and without SRL [In content equal to 0.0 in Fig. 10(c)] is compared one might conclude that the presence of the strain reducing layer influences mainly the positively charged exciton complex and the ground state energy, while the biexciton and negatively charged exciton binding energies remain almost constant. Thus, our theoretical study on the influence of the QD geometry as well as the average In content in both QDs and SRL shows that experimental results seen in Fig. 5(b) can be well reproduced mainly by tailoring the In content in SRL and QD rather than to QD geometry. Similarly in the experiment, the QDs with both  $X^-$  binding energy higher and lower compared to XX binding energy were observed evidencing that we are in the regime of their intercrossing as shown in Fig. 5(b). Comparison with theoretical calculations [Fig. 10(b)] proves that these effects are governed and rather sensitive to the average In composition in the QD. Furthermore, we observe that

smaller QDs with higher In content would be beneficial from the single-photon emitter application point of view (well-isolated optical transitions at telecom wavelengths), and would allow one to reach binding energies of the positive trion of up to -1.0 meV while keeping the emission wavelength within the 2<sup>nd</sup> telecommunication band.

## V. CONCLUSIONS

In this work, we examined experimentally and theoretically the electronic structure and optical properties of single strain-engineered InGaAs/GaAs QDs emitting in the telecom O-band at 1.3  $\mu\text{m}$ . The investigated structures exhibit a neutral exciton fine structure splitting of 65  $\mu\text{eV}$  on average and biexciton binding energies similar to common InGaAs/GaAs QDs emitting below 1  $\mu\text{m}$  on the level of -3.5 meV. Whereas there is no clear dependence on the neutral exciton emission energy, their interdependence points out that they are governed mostly by the In content in a QD. All excitonic complexes have a binding character with the binding energy of the positive trion in the range of -1 meV and that of the negative one around -3.6 meV. Both the higher energy excitonic spectrum (s-p splitting 75 meV) as well as the binding energies of excitonic complexes are well reproduced by the 8-band  $k \cdot p$  calculations combined with the configuration interaction method. Good quantitative agreement between the results of the experiment and the calculations was obtained by using a realistic, strongly inhomogeneous In distribution within the QD following the structural data. Additionally, the number of electron and hole basis states constituting the input for configuration interaction calculations has been varied proving the importance of correlation effects in the investigated system - the best results were obtained when 40 electron and 40 hole states were included. Whereas the In composition in both, the QD and the strain reducing layer, has strong impact on the exciton ground state transition energy and leads to the energy redshift towards the telecom range, the exact QD size nor the composition of the strain reducing layer do not influence the binding energies of the excitonic complexes predominantly. These are mostly determined by the In composition in the QD itself and with its increase the ordering of the excitonic complexes changes substantially in the emission spectra: the positive trion becomes less bound than the negative one, what makes the negative trion bound even stronger than the biexciton. As a result, the In composition can be used to tune the electronic properties of the InGaAs/GaAs QDs, but it has to be balanced between the QD and strain reducing layer to maintain the ground state emission energy in the telecom O-band.

## ACKNOWLEDGEMENTS

We thank Nora Schmitt and Prof. Michael Lehmann (Technical University of Berlin) for the TEM measurements. This work was funded by the FI-SEQR project jointly financed by the European Regional Development Fund (EFRE) of the European Union in the framework of the programme to promote research, innovation and technologies (Pro FIT) in Germany, and the National Centre for Research and Development in Poland within the 2nd Poland-Berlin Photonics Programme, grant No. 2/POLBER-2/2016 (project value 2 089 498 PLN). Support from the German Science Foundation via CRC 787 is also acknowledged.

## REFERENCES

- <sup>1</sup> F. Jahnke, *Quantum Optics with Semiconductor Nanostructures* (2012).

- <sup>2</sup> Ł. Dusanowski, M. Syperek, P. Mrowiński, W. Rudno-Rudziński, J. Misiewicz, A. Somers, S. Höfling, M. Kamp, J.P. Reithmaier, and G. Şek, *Appl. Phys. Lett.* **105**, 021909 (2014).
- <sup>3</sup> M. Benyoucef, M. Yacob, J.P. Reithmaier, J. Kettler, and P. Michler, *Appl. Phys. Lett.* **103**, 162101 (2013).
- <sup>4</sup> K. Takemoto, M. Takatsu, S. Hirose, N. Yokoyama, Y. Sakuma, T. Usuki, T. Miyazawa, and Y. Arakawa, *J. Appl. Phys.* **101**, 081720 (2007).
- <sup>5</sup> M.D. Birowosuto, H. Sumikura, S. Matsuo, H. Taniyama, P.J. van Veldhoven, R. Nötzel, and M. Notomi, *Sci. Rep.* **2**, 321 (2012).
- <sup>6</sup> K. Nishi, H. Saito, S. Sugou, and J.S. Lee, *Appl. Phys. Lett.* **74**, 1111 (1999).
- <sup>7</sup> V.M. Ustinov, N. A. Maleev, A. E. Zhukov, A. R. Kovsh, A. Y. Egorov, A. V. Lunev, B. V. Volovik, I.L. Krestnikov, Y.G. Musikhin, N. Bert, P.S. Kop'ev, Z.I. Alferov, N.N. Ledentsov, and D. Bimberg, *Appl. Phys. Lett.* **74**, 2815 (1999).
- <sup>8</sup> J. Bloch, J. Shah, W.S. Hobson, J. Lopata, and S.N.G. Chu, *Appl. Phys. Lett.* **75**, 2199 (1999).
- <sup>9</sup> L. Seravalli, M. Minelli, P. Frigeri, P. Allegri, V. Avanzini, and S. Franchi, *Appl. Phys. Lett.* **82**, 2341 (2003).
- <sup>10</sup> E.C. Le Ru, P. Howe, T.S. Jones, and R. Murray, *Phys. Status Solidi C Conf.* **1224**, 1221 (2003).
- <sup>11</sup> E. Goldmann, S. Barthel, M. Florian, K. Schuh, and F. Jahnke, *Appl. Phys. Lett.* **103**, 242102 (2013).
- <sup>12</sup> M.B. Ward, M.C. Dean, R.M. Stevenson, A.J. Bennett, D.J.P. Ellis, K. Cooper, I. Farrer, C. A. Nicoll, D.A. Ritchie, and A.J. Shields, *Nat. Commun.* **5**, 3316 (2014).
- <sup>13</sup> S. Maier, K. Berschneider, T. Steinl, A. Forchel, S. Höfling, C. Schneider, and M. Kamp, *Semicond. Sci. Technol.* **29**, 052001 (2014).
- <sup>14</sup> J. Kettler, M. Paul, F. Olbrich, K. Zeuner, M. Jetter, P. Michler, M. Florian, C. Carmesin, and F. Jahnke, *Phys. Rev. B* **94**, 045303 (2016).
- <sup>15</sup> A. Salhi, S. Alshaibani, B. Ilahi, M. Alhamdan, A. Alyamani, H. Albrithen, and M. El-Desouki, *J. Alloys Compd.* **714**, 331 (2017).
- <sup>16</sup> W.S. Liu, D.M.T. Kuo, J.I. Chyi, W.Y. Chen, H.S. Chang, and T.M. Hsu, *Appl. Phys. Lett.* **89**, 243103 (2006).
- <sup>17</sup> K. Akahane, N. Yamamoto, S. Gozu, A. Ueta, and N. Ohtani, *Phys. E Low-Dimensional Syst. Nanostructures* **32**, 81 (2006).
- <sup>18</sup> A. Hospodková, J. Pangrác, J. Vyskočil, M. Zíková, J. Oswald, P. Komninou, and E. Hulicius, *J. Cryst. Growth* **414**, 156 (2015).
- <sup>19</sup> N.N. Ledentsov, A.R. Kovsh, A.E. Zhukov, N.A. Maleev, S.S. Mikhlin, A.P. Vasil'ev, E.S. Semenova, M. V Maximov, Y.M. Shernyakov, N. V Kryzhanovskaya, V.M. Ustinov, and D. Bimberg, *Electron. Lett.* **39**, 1126 (2003).
- <sup>20</sup> L. Seravalli, G. Trevisi, P. Frigeri, D. Rivas, G. Muñoz-Matutano, I. Suárez, B. Alén, J. Canet, and J.P. Martínez-Pastor, *Appl. Phys. Lett.* **98**, 173112 (2011).

- <sup>21</sup> K. Shimomura and I. Kamiya, Appl. Phys. Lett. **106**, 082103 (2015).
- <sup>22</sup> S. Sengupta, S.Y. Shah, N. Halder, and S. Chakrabarti, Opto-Electronics Rev. **18**, 295 (2010).
- <sup>23</sup> M. A. Majid, D.T.D. Childs, K. Kennedy, R. Airey, R. A. Hogg, E. Clarke, P. Spencer, and R. Murray, Appl. Phys. Lett. **99**, 051101 (2011).
- <sup>24</sup> M.A. Majid, D.T.D. Childs, H. Shahid, R. Airey, K. Kennedy, R.A. Hogg, E. Clarke, P. Spencer, and R. Murray, Electron. Lett. **47**, 44 (2011).
- <sup>25</sup> M.B. Ward, O.Z. Karimov, D.C. Unitt, Z.L. Yuan, P. See, D.G. Gevaux, A.J. Shields, P. Atkinson, and D.A. Ritchie, Appl. Phys. Lett. **86**, 201111 (2005).
- <sup>26</sup> B. Alloing, C. Zinoni, V. Zwiller, L.H. Li, C. Monat, M. Gobet, G. Buchs, A. Fiore, E. Pelucchi, and E. Kapon, Appl. Phys. Lett. **86**, 101908 (2005).
- <sup>27</sup> R.P. Mirin, J.P. Ibbetson, J.E. Bowers, and A.C. Gossard, J. Cryst. Growth **175–176**, 696 (1997).
- <sup>28</sup> M. V Maximov, A.F. Tsatsul’nikov, B. V Volovik, D.S. Sizov, Y.M. Shernyakov, I.N. Kaiander, A.E. Zhukov, A.R. Kovsh, S.S. Mikhlin, V.M. Ustinov, Z.I. Alferov, R. Heitz, V.A. Shchukin, N.N. Ledentsov, D. Bimberg, Y.G. Musikhin, and W. Neumann, Phys. Rev. B **62**, 16671 (2000).
- <sup>29</sup> Y.D. Jang, N.J. Kim, J.S. Yim, D. Lee, S.H. Pyun, W.G. Jeong, and J.W. Jang, Appl. Phys. Lett. **88**, 231907 (2006).
- <sup>30</sup> Ł. Dusanowski, P. Holewa, A. Maryński, A. Musiał, T. Heuser, N. Srocka, D. Quandt, A. Strittmatter, S. Rodt, J. Misiewicz, and S. Reitzenstein, Opt. Express **25**, 340 (2017).
- <sup>31</sup> F. Guffarth, R. Heitz, A. Schliwa, O. Stier, N.N. Ledentsov, A.R. Kovsh, V.M. Ustinov, and D. Bimberg, Phys. Rev. B **64**, 85305 (2001).
- <sup>32</sup> E. Goldmann, M. Paul, F.F. Krause, K. Muller, J. Kettler, T. Mehrrens, A. Rosenauer, M. Jetter, P. Michler, and F. Jahnke, Appl. Phys. Lett. **105**, 1 (2014).
- <sup>33</sup> O. Stier, M. Grundmann, and D. Bimberg, Phys. Rev. B **59**, 5688 (1999).
- <sup>34</sup> A. Schliwa, G. Hönig, and D. Bimberg, *Multi-Band Effective Mass Approximations*, chapter 2, p. 57–86 (2014).
- <sup>35</sup> A. Schliwa, M. Winkelkemper, and D. Bimberg, Phys. Rev. B **79**, 075443 (2009).
- <sup>36</sup> F. Olbrich, J. Kettler, M. Bayerbach, M. Paul, J. Hörschele, S.L. Portalupi, M. Jetter, and P. Michler, J. Appl. Phys. **121**, 184302 (2017).
- <sup>37</sup> M. Paul, J. Kettler, K. Zeuner, C. Clausen, M. Jetter, and P. Michler, Appl. Phys. Lett. **106**, 122105 (2015).
- <sup>38</sup> C. Carmesin, F. Olbrich, T. Mehrrens, M. Florian, S. Michael, S. Schreier, C. Nawrath, M. Paul, J. Hörschele, B. Gerken, J. Kettler, S.L. Portalupi, M. Jetter, P. Michler, A. Rosenauer, and F. Jahnke, Phys. Rev. B **98**, 125407 (2018).
- <sup>39</sup> M. Paul, F. Olbrich, J. Hörschele, S. Schreier, J. Kettler, S.L. Portalupi, M. Jetter, and P. Michler, Appl. Phys. Lett. **111**, 033102 (2017).

- <sup>40</sup> F. Olbrich, J. Hörschle, M. Müller, J. Kettler, S. Luca Portalupi, M. Paul, M. Jetter, and P. Michler, *Appl. Phys. Lett.* **111**, 133106 (2017).
- <sup>41</sup> A. Maryński, P. Mrowiński, K. Ryczko, P. Podemski, K. Gawarecki, A. Musiał, J. Misiewicz, D. Quandt, A. Strittmatter, S. Rodt, S. Reitzenstein, and G. Sęk, *Acta Phys. Pol. A* **132**, 386 (2017).
- <sup>42</sup> P.-I. Schneider, N. Srocka, S. Rodt, L. Zschiedrich, S. Reitzenstein, and S. Burger, *Opt. Express* **26**, 8479 (2018).
- <sup>43</sup> N. Srocka, A. Musiał, P.-I. Schneider, P. Mrowiński, P. Holewa, S. Burger, D. Quandt, A. Strittmatter, S. Rodt, S. Reitzenstein, and G. Sęk, *AIP Adv.* **8**, 085205 (2018).
- <sup>44</sup> M. Sartison, L. Engel, S. Kolatschek, F. Olbrich, C. Nawrath, S. Hepp, M. Jetter, P. Michler, and S.L. Portalupi, *Appl. Phys. Lett.* **113**, 032103 (2018).
- <sup>45</sup> Y. Benny, Y. Kodriano, E. Poem, D. Gershoni, T.A. Truong, and P.M. Petroff, *Phys. Rev. B* **86**, 085306 (2012).
- <sup>46</sup> Y. Kodriano, E. Poem, N.H. Lindner, C. Tradonsky, B.D. Gerardot, P.M. Petroff, J.E. Avron, and D. Gershoni, *Phys. Rev. B* **82**, 155329 (2010).
- <sup>47</sup> E.R. Schmidgall, I. Schwartz, L. Gantz, D. Cogan, S. Raindel, and D. Gershoni, *Phys. Rev. B* **90**, 241411(R) (2014).
- <sup>48</sup> M. Wimmer, S. Nair, and J. Shumway, *Phys. Rev. B* **73**, 165305 (2006).
- <sup>49</sup> R.J. Young, R.M. Stevenson, A.J. Shields, P. Atkinson, K. Cooper, D.A. Ritchie, K.M. Groom, A. I. Tartakovskii, and M.S. Skolnick, *Phys. Rev. B* **72**, 113305 (2005).
- <sup>50</sup> M. Bayer, G. Ortner, O. Stern, A. Kuther, A. Gorbunov, A. Forchel, P. Hawrylak, S. Fafard, K. Hinzer, T. Reinecke, S.N. Walck, J.P. Reithmaier, F. Klopff, and F. Schäfer, *Phys. Rev. B* **65**, 195315 (2002).
- <sup>51</sup> A. Musiał, P. Gold, J. Andrzejewski, A. Löffler, J. Misiewicz, S. Höfling, A. Forchel, M. Kamp, G. Sęk, and S. Reitzenstein, *Phys. Rev. B* **90**, 045430 (2014).
- <sup>52</sup> V. Mlinar and A. Zunger, *Phys. Rev. B* **79**, 115416 (2009).
- <sup>53</sup> R. Seguin, A. Schliwa, S. Rodt, K. Potschke, U.W. Pohl, and D. Bimberg, *Phys. Rev. Lett.* **95**, 257402 (2005).
- <sup>54</sup> P.L. Ardel, K. Gawarecki, K. Müller, A.M. Waeber, A. Bechtold, K. Oberhofer, J.M. Daniels, F. Klotz, M. Bichler, T. Kuhn, H.J. Krenner, P. Machnikowski, and J.J. Finley, *Phys. Rev. Lett.* **116**, 077401 (2016).
- <sup>55</sup> C.E. Pryor, J. Kim, L.W. Wang, A.J. Williamson, and A. Zunger, *J. Appl. Phys.* **83**, 2548 (1998).
- <sup>56</sup> G. Bester, A. Zunger, X. Wu, and D. Vanderbilt, *Phys. Rev. B* **74**, 081305 (2006).
- <sup>57</sup> T.B. Bahder, *Phys. Rev. B* **41**, 11992 (1990).
- <sup>58</sup> K. Gawarecki, *ArXiv* 1711.06934 (2017).
- <sup>59</sup> V. Hernandez, J.E. Roman, and V. Vidal, *ACM Trans. Math. Softw.* **31**, 351 (2005).

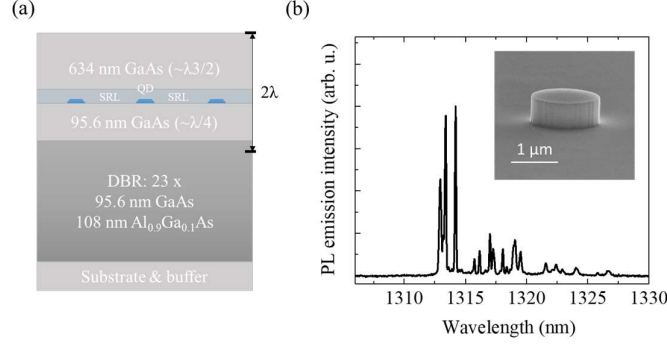


Fig. 1. (a) Sample layout of the investigated QD structure with GaAs substrate and buffer layer, 23 pairs of GaAs/ $\text{Al}_{0.9}\text{Ga}_{0.1}\text{As}$  to form the DBR, a single  $\text{In}_{0.75}\text{Ga}_{0.25}\text{As}$  QD layer on its wetting layer and embedded in an  $\text{In}_{0.2}\text{Ga}_{0.8}\text{As}$  strain reducing layer (SRL) and capped with a thick GaAs layer suitable for the fabrication of nanophotonic mesa structures with a  $2\lambda$  cavity. (b) High-resolution low-temperature microphotoluminescence spectrum of single QDs located in the  $1.5\ \mu\text{m}$  diameter mesa structure obtained under non-resonant excitation. To facilitate single-QD experiments a regular pattern of cylindrical mesas with varying diameters was fabricated using standard electron-beam lithography followed by reactive ion etching (inset: scanning electron microscope image of the investigated mesa structure).

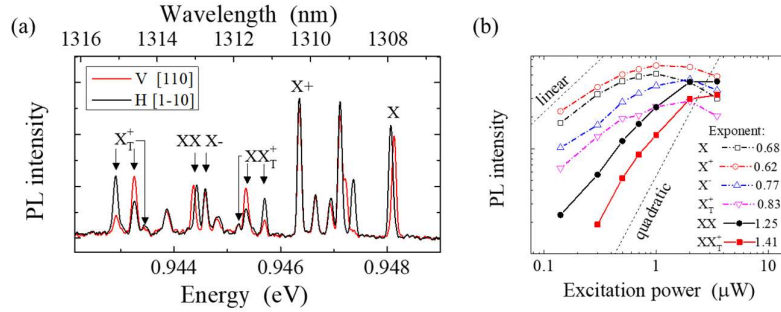


Fig. 2. (a) High-resolution low-temperature microphotoluminescence ( $\mu\text{PL}$ ) spectra from a single QD for two orthogonal linear polarization directions: along the  $[1-10]$  direction (black solid line) and  $[110]$  direction (red solid line) with various excitonic complexes marked as X (neutral exciton), XX (biexciton),  $X^+$  and  $X^-$  (positively and negatively charged excitons). Other spectral feature might be related to further excitonic complexes, those including carrier(s) in an excited state. Also, their origin from a second QD located in the same mesa cannot be excluded due to relatively high QD spatial density. (b) Analysis of the  $\mu\text{PL}$  emission intensity as a function of excitation power for the emission lines from (a).

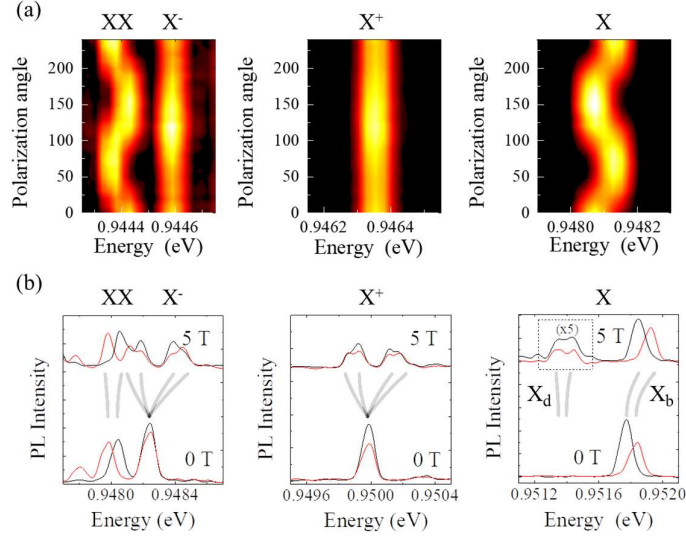


Fig. 3. (a) Polarization-resolved  $\mu$ PL showing the same fine structure splitting (FSS) for X (two bright excitons -  $X_b$ ) and XX with opposite polarizations as well as the lack of the FSS for  $X^+$  and  $X^-$ . (b)  $\mu$ PL spectra measured in magnetic field of 0 T and 5 T for two orthogonal linear polarizations showing the same quadruplet splitting of  $X^+$  and  $X^-$  as well as the dark exciton state  $X_d$ . The following system parameter values could be determined:  $g_{e,\perp} = 0.99$ ,  $g_{h,\perp} = 0.28$ ,  $\gamma = 2 \mu\text{eV/T}^2$ , exciton fine structure:  $\Delta E_{X_b} = 60 \mu\text{eV}$ ,  $\Delta E_{X_d} = 20 \mu\text{eV}$ ,  $\Delta E_{X_b-X_d} = 430 \mu\text{eV}$ .

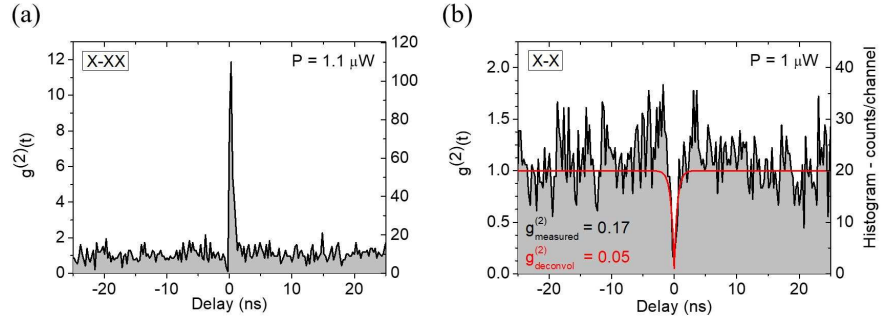


Fig. 4. (a) Cross-correlation of photon emission events for emission lines preliminary identified as XX and X (cf. Fig. 2 and 3) from a single QD, and (b) photon auto-correlation for the X emission line measured at 5 K under non-resonant cw excitation: black line – measurement data, red line – fit including convolution with the temporal resolution of the experimental setup (80 ps).

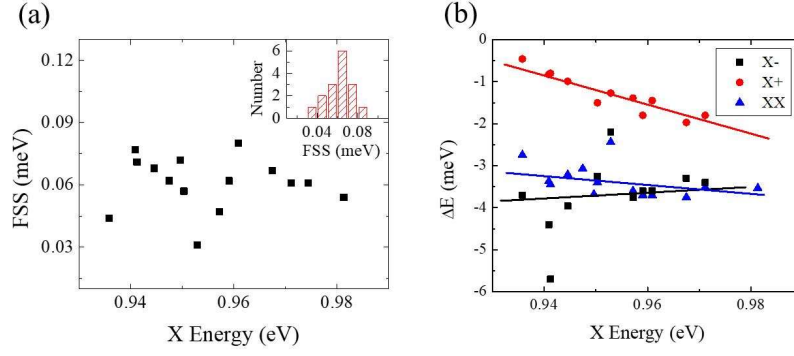


Fig. 5. Summary of the statistical measurements on more than 10 QDs: (a) Fine structure splitting (FSS) of the X (neutral exciton) as a function of X emission energy and FSS histogram (inset). (b) XX (biexciton),  $X^+$  (positive trion) and  $X^-$  (negative trion) binding energies as a function of X emission energy with solid lines providing guide to the eye.

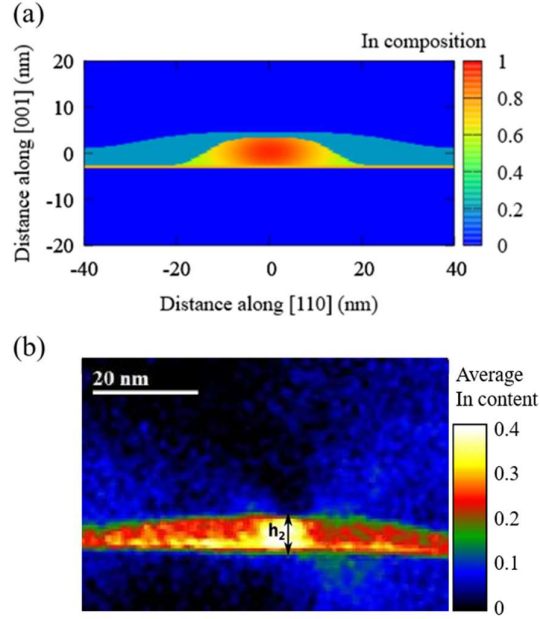


Fig. 6. (a) Applied model of a QD. The In composition  $\text{In}_x\text{Ga}_{1-x}\text{As}$  is color-coded. (b) Composition Evaluation by Lattice Fringe Analysis (CELFA) image from TEM measurement of the representative InGaAs/GaAs QD taken upon rotation of the sample by  $2\text{--}4^\circ$  out of [010] plane with the color scale referring to In content averaged over the sample thickness (see text for interpretation of the signal). Strongly inhomogeneous In distribution within the nanostructure volume is clearly visible.

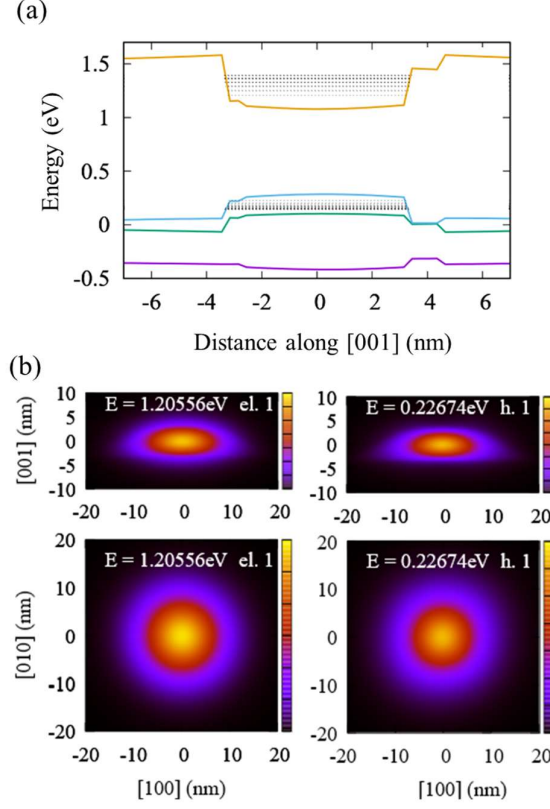


Fig. 7. (a) Single-particle levels (dotted lines) calculated within the 8-band k.p model with the band edge along the growth direction marked for the conduction band (yellow solid line) and for the valence subbands: blue, green and purple for heavy holes, light holes and spin-orbit split-off band, respectively. (b) Probability density of the carrier distribution for the first hole (right column) and electron (left column) levels for cross sections along the growth-direction (upper panel) and in-plane (lower panel) through the center of the QD.

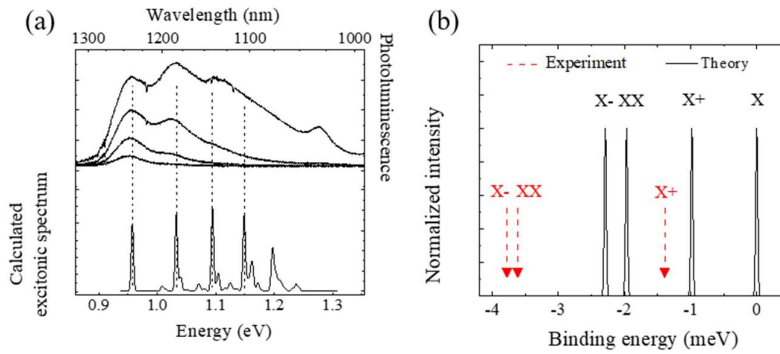


Fig. 8. (a) Photoluminescence spectra of the QD ensemble for increasing excitation power exhibiting the state filling effect with higher energy states clearly resolved (upper panel) compared to the calculated excitonic spectrum (lower panel). (b) Calculated single QD spectrum (black solid line) and experimental values of the spectrum (red dashed line) showing the binding energy (meV) versus normalized intensity.

binding energies of the excitonic complexes (red arrows). The energy of the neutral exciton from experiment and calculations coincides and it is subtracted from the results.

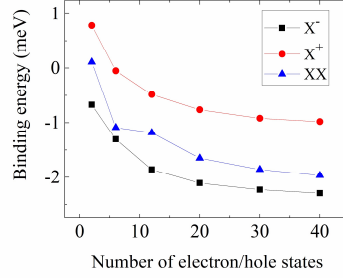


Fig 9. Influence of the number of electron/hole basis states included in the configuration interaction calculations on the binding energies of the basic excitonic complexes: positively ( $X^+$ ) and negatively charged ( $X^-$ ) trion and biexciton ( $XX$ ).

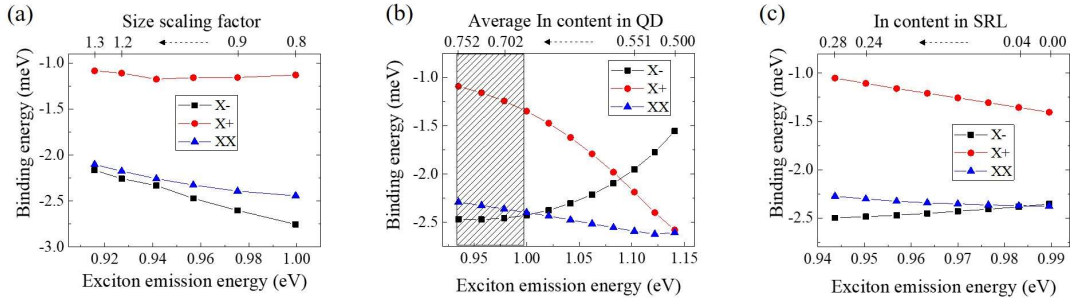


Fig 10. Results from calculations within the 8 band  $k$ - $p$  model combined with the configuration interaction method for binding energies of excitonic complexes as a function of: (a) QD size – the height to base size ratio is kept constant so the size scaling factor (SSF) represents the multiplications factor for dimensions in both directions; (b) average In content in the QD and (c) In content in the InGaAs strain reducing layer (SRL). The data are presented in dependence on the exciton emission energy. Nominal fixed parameters: (a) QD  $r_b$ : 15 nm x SSF, QD  $h$ : 6 nm x SSF, average In content in QD: 73 %, In content in SRL: 20 %, (b) QD  $r_b$ : 15 nm,  $h$ : 6 nm, In content in SRL: 20 %, (c) QD  $r_b$ : 15 nm,  $h$ : 6 nm, average In content in QD: 73 %. The marked region in (b) corresponds to the energy range of experimental data available in the investigated sample. In the case of (a) and (c) the energy ranges are similar for both theoretical calculations and experimental data.